Cerebral Cortex, November 2020;30: 5830–5843

doi: 10.1093/cercor/bhaa160
Advance Access Publication Date: 17 June 2020
Original Article

ORIGINAL ARTICLE

Connections of the Human Orbitofrontal Cortex and Inferior Frontal Gyrus

Chih-Chin Heather Hsu[1], Edmund T. Rolls[2,3,4], Chu-Chung Huang[2], Shin Tai Chong[5], Chun-Yi Zac Lo[2], Jianfeng Feng[3,4,7] and Ching-Po Lin[1,2,5,6]

[1]Department of Biomedical Imaging and Radiological Sciences, National Yang-Ming University, Taipei 11221, Taiwan, [2]Institute of Science and Technology for Brain Inspired Intelligence, Fudan University, Shanghai 200433, China, [3]Department of Computer Science, University of Warwick, Coventry CV4 7AL, UK, [4]Oxford Centre for Computational Neuroscience, Oxford, UK, [5]Institute of Neuroscience, National Yang-Ming University, Taipei 11221, Taiwan, [6]Brain Research Center, National Yang-Ming University, Taipei 11221, Taiwan and [7]Key Laboratory of Computational Neuroscience and Brain-Inspired Intelligence (Fudan University), Ministry of Education, 200433, China

Address correspondence to Professor Edmund T. Rolls, Department of Computer Science, University of Warwick, Coventry CV4 7AL, UK. Email: Edmund.Rolls@oxcns.org; Professor Jianfeng Feng, Institute of Science and Technology for Brain-inspired Intelligence, School of Mathematical Sciences, Fudan University, Shanghai 200433, China. Email: jianfeng64@gmail.com; Professor Ching-Po Lin, Institute of Neuroscience, National Yang-Ming University, Taipei 11221, Taiwan. Email: chingpolin@gmail.com.

Abstract

The direct connections of the orbitofrontal cortex (OFC) were traced with diffusion tractography imaging and statistical analysis in 50 humans, to help understand better its roles in emotion and its disorders. The medial OFC and ventromedial prefrontal cortex have direct connections with the pregenual and subgenual parts of the anterior cingulate cortex; all of which are reward-related areas. The lateral OFC (OFClat) and its closely connected right inferior frontal gyrus (rIFG) have direct connections with the supracallosal anterior cingulate cortex; all of which are punishment or nonreward-related areas. The OFClat and rIFG also have direct connections with the right supramarginal gyrus and inferior parietal cortex, and with some premotor cortical areas, which may provide outputs for the OFClat and rIFG. Another key finding is that the ventromedial prefrontal cortex shares with the medial OFC especially strong outputs to the nucleus accumbens and olfactory tubercle, which comprise the ventral striatum, whereas the other regions have more widespread outputs to the striatum. Direct connections of the OFC and IFG were with especially the temporal pole part of the temporal lobe. The left IFG, which includes Broca's area, has direct connections with the left angular and supramarginal gyri.

Key words: connections, diffusion tractography imaging, emotion, inferior frontal gyrus, orbitofrontal cortex

Introduction

The orbitofrontal cortex (OFC) is a key brain region involved in emotion (Rolls 2014, 2019b). Part of its importance in emotion is that the human OFC encodes reward value and pleasantness in the medial OFC, and punishment value, unpleasantness, and nonreward in the lateral OFC (Rolls 2019c). The ventromedial prefrontal cortex is also involved in emotion and may be especially involved in emotion-related decision-making, based on the activations in it during reward-related decision-making (Rolls and Grabenhorst 2008; Rolls et al. 2010b, 2010a; Grabenhorst and Rolls 2011) and the effects of damage to it on decision-making (Hornak et al. 2004; Wheeler and Fellows 2008; Glascher et al. 2012). It is important to understand the functioning of these regions better, for all are implicated, in different ways, in depression by their altered functional connectivity (Cheng et al. 2016; Cheng, Rolls, Qiu, Xie, Wei,

et al. 2018b; Cheng, Rolls, Qiu, Yang, et al. 2018c; Cheng, Rolls, Ruan, et al. 2018d; Rolls, Cheng, et al. 2020a). Furthermore, in depression, at least the orbital part of the right inferior frontal gyrus (rIFG) has similarly altered functional connectivity to that of the immediately adjacent lateral OFC (Rolls, Cheng, et al. 2020a).

To understand the functioning of a brain region, it is very important to know where it receives its inputs from and where it projects to (Rolls 2016a, 2021). There is a wealth of evidence on this in nonhuman primates, in which anatomical pathways can be traced (Carmichael and Price 1996; Price 2006; Price 2007; Saleem et al. 2008; Saleem et al. 2014). However, these methods cannot be applied in humans, and there is a little evidence on the direct connections of the OFC, ventromedial prefrontal cortex, and inferior frontal gyrus in humans. Some of the evidence available on the connectivity of these regions in humans comes from studies of functional connectivity (Du et al. 2020). Functional connectivity, measured by correlations in the BOLD signal between pairs of brain regions, does reflect direct connections as shown by combined anatomical and functional connectivity studies in nonhuman primates but also reflects trans-synaptic effects (Van Essen et al. 2019).

Given this background, the aim of the present investigation was to use diffusion tractography imaging to investigate the direct connections of the human OFC, ventromedial prefrontal cortex, and inferior frontal gyrus. These three brain regions were all included in this investigation because parts of all of them are related to emotion and depression (Rolls 2019b, 2019c; Rolls, Cheng, et al. 2020a), and we wished to know to what extent different parts of these areas have related or different connectivity. Diffusion tractography imaging, which is an MRI method that can probe direction-dependent diffusivity of water molecules in fiber bundles, can provide evidence on direct connections between brain regions (Mori and van Zijl 2002; Johansen-Berg et al. 2005; Donahue et al. 2016). Some previous studies have used tractography to investigate the connectivity of some limbic areas (Catani et al. 2013; Folloni et al. 2019) including the subgenual cingulate cortex (Johansen-Berg et al. 2008), but this is the first study we know to focus on the human OFC, ventromedial prefrontal cortex, and inferior frontal gyrus; to include a large number ($N = 50$) of participants in such a study to allow statistical evaluation of the connections of these brain areas with all other areas of the cerebrum; and to analyze the results in a way that facilitates comparison with the functional connectivity of the same brain areas (Du et al. 2020). We emphasize that this is a voxel-level direct connectivity study, but a feature is that the regions are identified by the automated anatomical labelling atlas 3 (AAL3), which has a useful parcellation of both the orbitofrontal and anterior cingulate cortices (Rolls et al. 2015; Rolls, Huang, et al. 2020b).

Methods

Participants

Data from 50 healthy aging participants (M/F = 19/31, mean age = 64.3 ± 6.0, education = 14.6 ± 2.8 year) from the Longitudinal Aging Study of Taipei (LAST) were analyzed in this study. LAST is a community-based aging cohort study conducted in Taipei and new Taipei city of Taiwan. The inclusion criteria for LAST participants were: 1) inhabitants of Taipei or new Taipei city without a plan to move in the near future and 2) residents aged 50 years or older. People with the following conditions were excluded: 1) unable to communicate and complete an interview; 2) unable to complete all tests due to poor functional status; 3) those who had a limited life expectancy due to major illnesses; and 4) those who were currently institutionalized. All participants signed a written informed consent agreement before they were enrolled for study. The study was approved by the Institutional Review Board of the National Yang Ming University, Taipei, Taiwan. All participants received the Montreal Cognitive Assessment (MoCA) for the global cognitive functional neuropsychological assessment, which is an alternative for the Mini-Mental State Exam (MMSE) that better identifies cognitive deficits in participants over 60 years old than MMSE (Nasreddine et al. 2005). MoCA scores range between 0 and 30. A score of 26 or over is considered to be normal. In this study, the participants' average MoCA score was 27.64 ± 1.92 (±SD).

MRI Acquisition

All neuroimaging was performed on a 3 T MR scanner (Siemens Magnetom Tim Trio, Erlangen, Germany) at the National Yang-Ming University, using a 12-channel head array coil. High-resolution T_1-weighted (T1W) MR images were acquired using a 3D Magnetization-Prepared Rapid Gradient Echo sequence (TR/TE = 2530/3.5 ms, TI = 1100 ms, FOV = 256 mm, flip angle = 7°, matrix size = 256 × 256, 192 sagittal slices, slice thickness = 1 mm, no gap) for image segmentation, registration, and brain mask extraction. Multishelled, multiband diffusion weighted images (DWIs) were acquired using a single shot spin-echo planar imaging sequence (monopolar scheme, TR = 3525 ms, TE = 109.2 ms, Matrix size: 110 × 110, voxel size: 2 × 2 × 2 mm^3, multiband factor = 3, phase encoding: anterior to posterior) with two *b*-values of 1000 s/mm^2 (30 diffusion directions) and 3000 s/mm^2 (60 diffusion directions), in which b0 images were interleaved in every six volumes. Each volume consisted of 72 contiguous axial slices (thickness: 144 mm). Data with the same DWI protocol using an opposite polarity (phase encoding from posterior to anterior) were also acquired.

Diffusion MRI Preprocessing and Tractography

To correct for susceptibility-induced off-resonance field, image distortion induced by the fast-switching gradient, and slight head motion, FMRIB's Software Library (FSL) functions: TOPUP and EDDY were performed on DWIs with two opposite polarities (anterior and posterior). To reconstruct white matter (WM) tracts by using tractography imaging, first, T1W images were segmented into five tissue types, using 5TT (MRtrix3 command: 5ttgen) including cortical gray matter (GM), subcortical GM, WM, cerebrospinal fluid, and pathological tissue, in order to anatomically constrain the tractography terminations in GM. Whole brain tractography was reconstructed for each subject in native space. A Multi-Shell Multi-Tissue Constrained Spherical Deconvolution (MSMT-CSD) model with lmax = 8 and prior co-registered 5tt image was used on the preprocessed multishell DWI data to obtain the fiber orientation density (FOD) function (Smith 2002; Jeurissen et al. 2014). Based on the voxel-wise fiber orientation distribution, anatomically constrained tractography (ACT) using the iFOD2 algorithm was applied with random seeding of all WM voxels (20 seeds per voxel) to explore all possible connections without using a prior region of interest (ROI) for a hypothesis (Tournier et al. 2010; Smith et al. 2012). Placing seeds throughout the WM mask guaranteed that the reconstructed fibers would cover the whole of WM and that

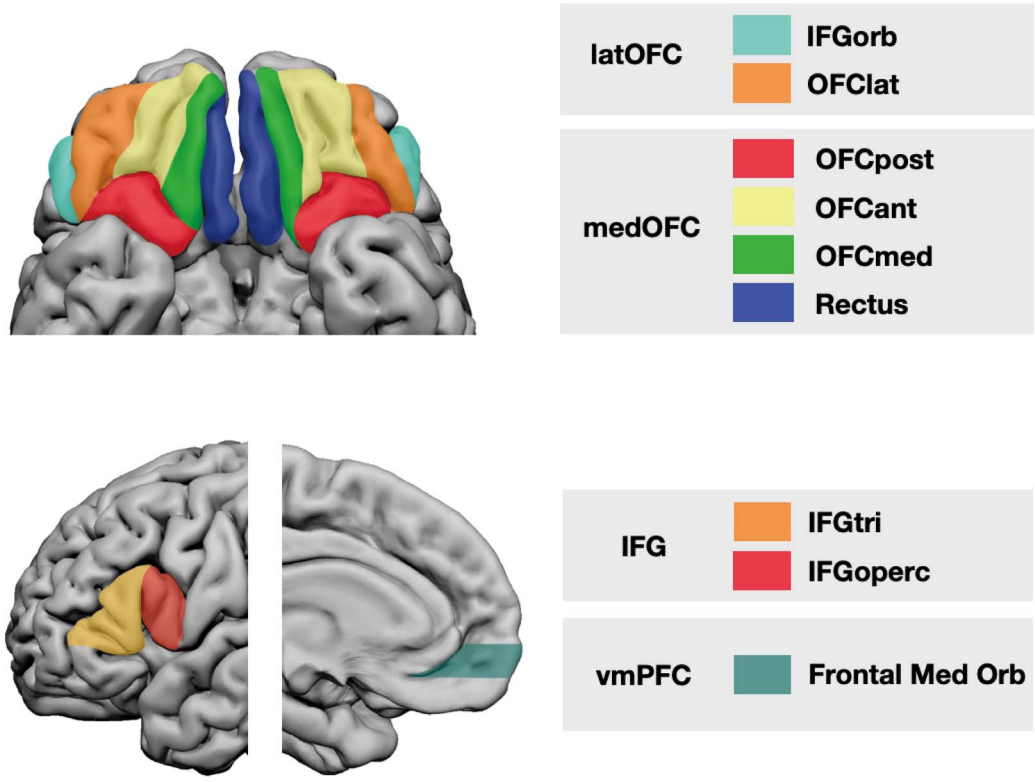

Figure 1. The four ROIs and the AAL3 areas included in each. The ventromedial prefrontal cortex ROI (vmPFC) is AAL3 area FrontalMedOrb; the medial OFC ROI (medOFC) consists of AAL3 areas gyrus rectus, OFCmed, OFCant, and OFCpost; the lateral OFC ROI (latOFC) consists of AAL3 OFClat and IFGorb; and the inferior frontal gyrus ROI (IFG) consists of AAL3 areas IFGtri (BA45) and IFGoperc (BA44). There is a close relation of these AAL3 areas (Rolls et al. 2015; Rolls, Huang, et al. 2020b) to the underlying cytoarchitecture (Öngür et al. 2003), with gyrus rectus corresponding to 14r; OFCmed to 13m; OFC post to 13l; OFCant to 11l; OFC lat to 12; OFGorb to the inferior frontal convexity which joins the lateral OFC 12 to the inferior frontal gyrus, 45; IFGtri to area 45; and IFGoperc to area 44. There is also a good correspondence of the AAL3 areas to the divisions of the OFC based on the parcellation of the functional connectivity (Du et al. 2020).

WM seeding captures more underlying streamlines between regions than seeding in a GM ROI (Zajac et al. 2017). To enhance the validity of the reconstructed fibers, the aforementioned 5TT was utilized as prior information during the tracking, and six mandatory rules were applied: 1) a streamline was terminated and accepted when it entered GM. 2) A streamline was rejected if it entered CSF. 3) A streamline was terminated and accepted if it left the FOV or user-defined brain mask. (This is necessary to permit tracts to include the spinal column.) 4) A streamline was terminated and rejected when it reached a voxel with a very low FOD amplitude or showed excessive curving angle in the WM (with default threshold: FOD amplitude 0.05 and curve angle 45°). 5) A streamline was accepted when rule (4) applied within subcortical regions. 6) A streamline was not allowed to exit subcortical GM and was truncated when it reached a minimum FOD amplitude within voxels of the subcortical GM (Smith et al. 2012). Whole-brain tractography was used for connectome reconstruction. To show the connectivity pattern of an ROI based on this voxel-to-voxel level connectivity, we included all voxel-to-voxel streamlines that terminated in the ROI.

In this study, we used the AAL3 (Rolls, Huang, et al. 2020b) (see Supplementary Tables S1 and S2 for description and abbreviations) to delineate individual brain areas of interest, because it has several divisions of the anterior cingulate cortex, as well as of the OFC areas introduced in AAL2 (Rolls et al. 2015). To transform the AAL3 atlas from MNI standard space to the individual native space, T1W images were first co-registered with null diffusion images ($b = 0$) using boundary-based registration to generate the transformation matrix from DWI-space to T_1-space (Greve and Fischl 2009). Second, T1W images were then spatially normalized to the MNI152 T1 template in standard space via linear affine transformation (FLIRT) and nonlinear registration (FNIRT) (Jenkinson and Smith 2001; Jenkinson et al. 2002). By combining the two transformation matrices (DWI to T1 and T1 to MNI), we then applied the inverse transformation matrix to obtain the AAL3 volumes in each individual's native DWI space with nearest neighbor interpolation. All the spatial registration and normalization procedures were implemented in FSL (http://www.fmrib.ox.ac.uk/fsl). In this study, we focused on the connectivity of eight ROIs which were defined by 18 AAL3 areas as shown in Figure 1 as follows, separately for the left and right: the ventromedial prefrontal cortex (vmPFC, AAL3 FrontalMedOrb); medial OFC (medOFC, AAL3 OFCpost, OFCant, OFCmed, and rectus); lateral OFC (latOFC, AAL3 OFClat, and IFGorb); and inferior frontal gyrus (IFG, IFGtri, and IFGoperc). The left and right were analyzed separately, because there is evidence supporting the asymmetry of the connectivity in the left and right IFG (Du et al. 2020), and to provide evidence on the extent to which each of the ROIs has bilateral

connections. To reduce potential false positive tracts generated by seeding in only a few specific regions, whole-brain tractography was performed and the connectivity profiles of the ROIs were then extracted. With the native-space AAL3 atlas, we used the tck2connectome command to generate the connectivity matrix for whole-brain tractography, in which a 2-mm radial search was applied to each streamline endpoint to locate the nearest node. The number of streamline fibers between pairs of AAL3 brain regions was measured across the 140 brain regions (the 26 regions of the cerebellum were omitted from the analyses). The number of streamlines between brain regions was then normalized by the average size (number of voxels) of each ROI pair to reduce the bias toward capturing more streamlines between large ROI pairs. Thus, the connectivity for different ROI pairs was evaluated by the normalized number of streamlines (fibers per voxel). This enabled us to produce a matrix of the connectivity between each of the OFC/inferior frontal gyrus ROIs and every other AAL3 area. (An example is in Figure 4).

To establish the termination map of streamline tracts throughout the brain for individual subjects, we extracted the coordinates of every fiber termination identified for each of the eight ROIs and recorded the number of connections to obtain the voxel-wise connection patterns in native space. The native termination maps were than warped into the MNI standard space for further representation and statistical analyses. (Examples of such maps are shown in Fig. 2 and Supplementary Fig. S1).

Statistics

To investigate the connectivity patterns of fiber projections between each of the 18 AAL3 areas in the eight ROIs (left and right: vmPFC [AAL3 FrontalMedOrb], medial OFC [Rectus, OFCmed, OFCant, and OFCpost], lateral OFC [OFClat and IFGorb], and Inferior Frontal Gyrus [IFGoperc and IFGtri]) and each AAL3 region throughout the brain, the following statistical analysis was performed. For each of the 50 participants, the background level of normalized streamlines between each of the 18 AAL3 areas and each of the early visual cortical areas was measured. The early visual areas, Calcarine to OccipitalInf in the AAL3 atlas (AAL3 47–58), were used as control regions, because based on known anatomy in macaques (Carmichael and Price 1996; Price 2006, 2007; Saleem et al. 2008, 2014), there are unlikely to be direct connections between these OFC ROIs and early visual cortical areas. The mean background level across visual cortical areas provided a background measure for each of the 18 AAL3 areas for each participant. Then, a paired *t*-test was performed across the 50 subjects for each link between AAL3 regions and the 18 AAL3 areas in the four ROIs to test whether the normalized number of streamlines was greater than the baseline background measure, using Bonferroni correction (corrected P-value < 0.05) for multiple comparisons across all AAL3 areas (140). (This resulted in an analysis of the type illustrated in Fig. 4 and Supplementary Fig. S2).

To show the voxel-level connectivity patterns of the eight ROIs across the 50 participants, a paired *t*-test was also used to examine whether the number of streamline terminations in each voxel was significantly greater than the mean number of terminations for the baseline background. Termination *t* maps in MNI standard space were generated for the voxel-wise connectivity of the eight ROIs, using a threshold *t* value for $P < 0.001$ uncorrected, to produce analyses of the type illustrated in Figure 3.

Results

Connectivity of Different Regions of the OFC and Nearby Areas for a Typical Single Subject

We start by showing in Figure 2 and Supplementary Figure S1 for two single subjects the streamline terminations throughout the brain for five different ROIs, the right ventromedial prefrontal cortex, right medial OFC, right lateral OFC, and left and right IFG. Separate diagrams are provided for the left and right IFG because the connectivity of the IFG was asymmetric between the right and left hemispheres, whereas for the other brain regions, the connectivity was symmetric. The connectivity for each of these five brain regions is described next. We emphasize that this is a voxel-level connectivity study. The AAL3 atlas is used only to delineate areas to which we wish to refer. The AAL3 regions that were the origin/termination of the streamlines in the ROIs are shown in Figure 1. The streamlines for the second typical subject are shown in Supplementary Figure S1 to indicate the robustness even at the single subject level, are shown with more coronal slices, and are drawn on for the following description.

Ventromedial Prefrontal Cortex

Figure 2A and Supplementary Figure S1A show the streamline terminations for the ventromedial prefrontal cortex. Terminations are evident in the frontal pole, lateral OFC, medial OFC, striatum (ventral striatum and parts of the caudate and putamen), temporal pole, dorsolateral amygdala (with the streamline terminations there at $Y = 0$ probably indicating where the following of the streamlines terminates as bundles enter the amygdala), inferior temporal cortex (with sparse connectivity illustrated), and the posterior cingulate cortex (at $Y = -42$). We note that it is typically not possible to easily follow the streamline tracts from the WM into the GM of the cortex itself because there are so many axons running tangentially just below layer 6 of the cortex, connecting to other cortical regions. These tangential fibers produce difficulty in following the diffusion-based process that is present in the streamlined fibers being traced (Van Essen, personal communication, 2019).

Medial OFC

Figure 2B and Supplementary Figure S1B show the streamline terminations for the medial OFC. Terminations are evident in the frontal pole, lateral OFC, pregenual cingulate cortex (with less connectivity to the supracallosal anterior cingulate cortex), striatum (ventral striatum, caudate, and putamen), temporal pole, dorsolateral amygdala, middle and inferior temporal gyrus, the posterior cingulate cortex (at $Y = -36$ to $Y = -48$), and precuneus ($Y = -48$ to $Y = -66$). Interestingly, some connectivity to contralateral OFC areas is evident.

Lateral OFC

Figure 2C and Supplementary Figure S1C show the streamline terminations for the lateral OFC. Terminations are evident in the frontal pole and dorsolateral prefrontal cortex, medial OFC, inferior frontal gyrus, supracallosal anterior cingulate cortex ($Y = 12$ to $Y = 18$, with less connectivity to the pregenual cingulate cortex), anterior insula ($Y = 12$ to $Y = 18$), premotor cortex ($Y = 0$ to $Y = 6$), striatum (ventral striatum, caudate, and putamen), temporal pole, dorsolateral amygdala, inferior temporal cortex, the posterior cingulate cortex (at $Y = -36$ to $Y = -48$), precuneus ($Y = -48$ to $Y = -66$), the angular gyrus (at $Y = -36$), and the MDm (the magnocellular part of the mediodorsal nucleus of the thalamus).

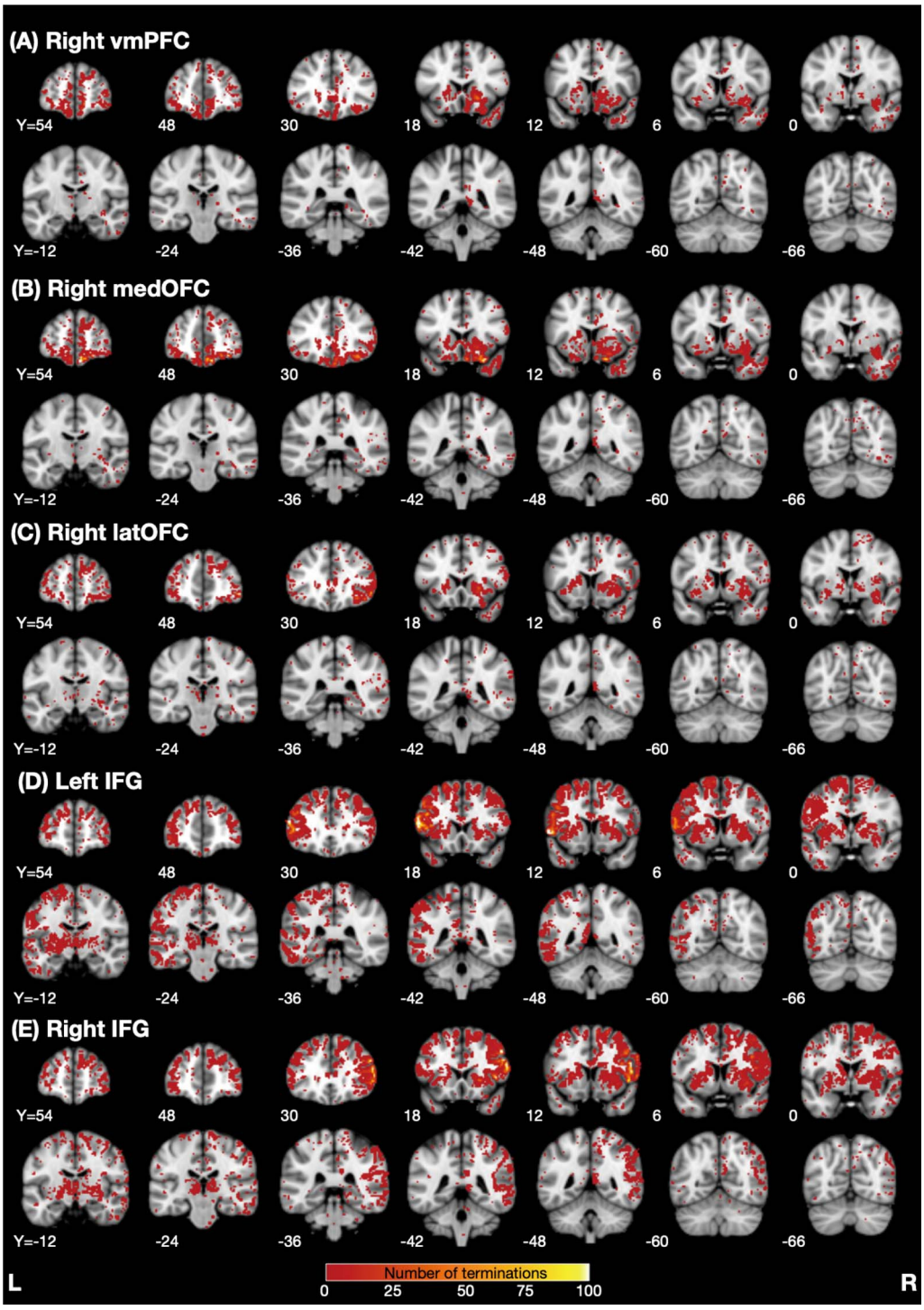

Figure 2. The regions with streamline terminations for the connectivity of different regions of the OFC and nearby areas for a typical single subject shown in MNI space. Separate subdiagrams are provided for the (*A*) right ventromedial prefrontal cortex, (*B*) right medial OFC, (*C*) right lateral OFC, and (*D*) left and (*E*) right IFG.

Left Inferior Frontal Gyrus

Figure 2*D* and Supplementary Figure S1*D* show the streamline terminations for the left inferior frontal gyrus. Terminations are evident in the frontal pole and superior, and middle frontal gyri, supracallosal anterior cingulate cortex ($Y = 12$ to $Y = 18$, with little connectivity to the pregenual cingulate cortex), anterior insula ($Y = 12$ to $Y = 18$), premotor cortex ($Y = 0$ to $Y = 6$), striatum (caudate, putamen, and ventral striatum), temporal pole, dorsolateral amygdala, inferior temporal (visual) cortex, superior temporal (auditory) cortex ($Y = -12$ to $Y = -24$), the posterior cingulate cortex (at $Y = -36$ to $Y = -48$), precuneus ($Y = -48$ to $Y = -66$), the left supramarginal gyrus area 40 (at $Y = -36$), the left angular gyrus area 39 (at $Y = -60$ to $Y = -66$), parietal area 7 (at $Y = -36$), and the thalamus. It is notable that there was

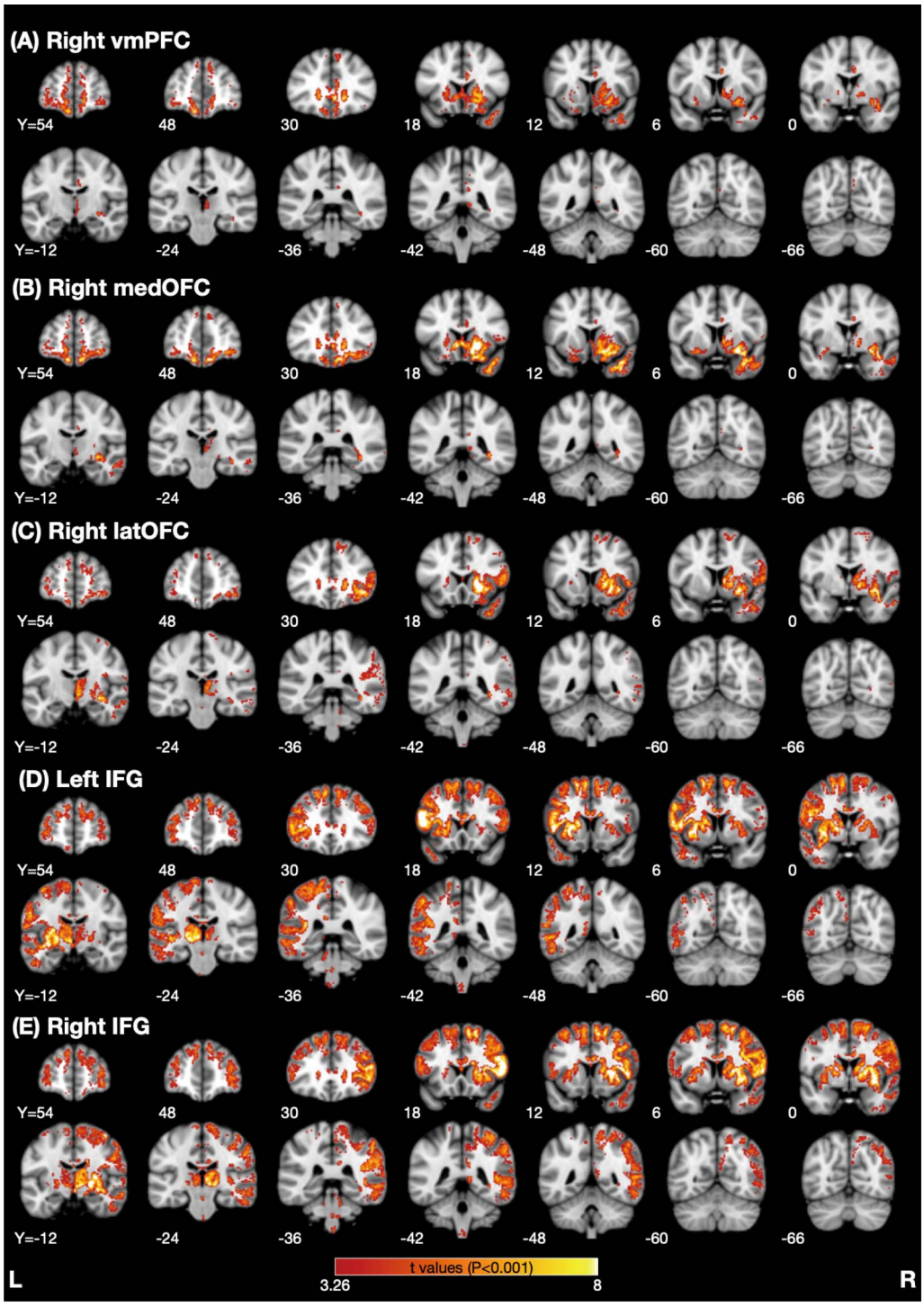

Figure 3. *t* maps from all 50 subjects to illustrate the strength of the connectivity of the OFC and related areas with other brain regions. Termination maps were examined by a voxel-wise paired *t* test using the mean termination numbers in the primary visual cortex as a baseline background measure with a statistical threshold of $P < 0.001$ uncorrected. Separate subdiagrams are provided for (*A*) the ventromedial prefrontal cortex, (*B*) medial OFC, (*C*) lateral OFC, and (*D*) left and (*E*) right IFG.

little connectivity with the medial OFC, ventromedial prefrontal cortex, and pregenual cingulate cortex.

Right Inferior Frontal Gyrus

Figure 2E and Supplementary Figure S1E show the streamline terminations for the rIFG. Terminations are evident in the frontal pole and superior, and middle frontal gyri, lateral OFC ($Y = 30$), supracallosal anterior cingulate cortex ($Y = 12$ to $Y = 30$, with little connectivity to the pregenual cingulate cortex), anterior insula ($Y = 12$ to $Y = 18$), premotor cortex ($Y = 0$ to $Y = 6$), striatum (caudate, putamen, and ventral striatum), temporal pole, dorsolateral amygdala, inferior temporal (visual) cortex, middle

temporal gyrus, superior temporal (auditory) cortex (Y = −12 to Y = −24), the posterior cingulate cortex (at Y = −36 to Y = −48), precuneus (Y = −48 to Y = −66), the right supramarginal gyrus area 40 (at Y = −36), the right angular gyrus area 39 (at Y = −60 to Y = −66), parietal area 7 (at Y = −36), and the thalamus. It is notable that there was a little connectivity with the medial OFC, ventromedial prefrontal cortex, and pregenual cingulate cortex.

The Statistics of the Connectivity of the OFC and Related ROIs with Voxels in Other Brain Regions Analyzed Across 50 Participants

Figure 3 shows *t* maps from all 50 subjects to illustrate the strength of the connectivity of the OFC and related areas with other brain regions, as described in Materials and Methods. Termination maps were examined using a one-sample *t* test with a statistical threshold of $P < 0.001$ uncorrected as described in Materials and Methods.

Ventromedial Prefrontal Cortex

Figure 3A shows the *t* maps for the streamline terminations for the ventromedial prefrontal cortex. The terminations are most significant in the frontal pole, lateral and medial OFC, pregenual and subgenual cingulate cortex, striatum (ventral striatum, caudate, and putamen), temporal pole, dorsolateral amygdala, and the MDm (the magnocellular part of the mediodorsal nucleus of the thalamus).

Medial OFC

Figure 3B shows the *t* maps for the streamline terminations for the medial OFC. The terminations are most significant in the frontal pole, lateral OFC, pregenual cingulate cortex (Y = 30, with less connectivity to the supracallosal anterior cingulate cortex), striatum (ventral striatum, caudate, and putamen), temporal pole and inferior temporal cortex, dorsolateral amygdala, a region close to where connections may enter the hippocampal formation (Y = −12), and the MDm (the magnocellular part of the mediodorsal nucleus of the thalamus).

Lateral OFC

Figure 3C shows the *t* maps for the streamline terminations for the lateral OFC. The terminations are most significant in the frontal pole, medial OFC, anterior insula (Y = 12 to Y = 18), striatum (caudate, putamen, and ventral striatum), temporal pole and inferior temporal cortex, dorsolateral amygdala, the supramarginal gyrus (at Y = −36), and the MDm (the magnocellular part of the mediodorsal nucleus of the thalamus).

Left Inferior Frontal Gyrus

Figure 3D shows the z maps for the streamline terminations for the left inferior frontal gyrus. The terminations are most significant in the frontal pole and superior and middle frontal gyri, supracallosal anterior cingulate cortex (Y = 12 to Y = 18, with little connectivity to the pregenual cingulate cortex), anterior insula (Y = 12 to Y = 18), premotor cortex (Y = 0 to Y = 6), striatum (caudate, putamen, and ventral striatum), temporal pole, dorsolateral amygdala, inferior temporal (visual) cortex, superior temporal (auditory) cortex (Y = −12 to −24), the left supramarginal gyrus area 40 (at Y = −36), the left angular gyrus area 39 (at Y = −60 to −66), parietal area 7 (at Y = −36), and the thalamus. It is notable that there was a little connectivity with the medial OFC, ventromedial prefrontal cortex, and pregenual cingulate cortex.

Right Inferior Frontal Gyrus

Figure 3E shows the z maps for the streamline terminations for the rIFG. The terminations are most significant in the frontal pole and superior and middle frontal gyri, right lateral OFC (Y = 30), supracallosal anterior cingulate cortex (Y = 12 to Y = 18, with little connectivity to the pregenual cingulate cortex), anterior insula (Y = 12 to Y = 18), premotor cortex (Y = 0 to Y = 6), striatum (caudate, putamen, and ventral striatum), temporal pole, right inferior temporal (visual) cortex, middle temporal gyrus, superior temporal (auditory) cortex (Y = −12 to Y = −24), the right supramarginal gyrus area 40 (at Y = −36), the right angular gyrus area 39 (at Y = −60 to −66), parietal area 7 (at Y = −36), and the thalamus. It is notable that there was a little connectivity with the medial OFC, ventromedial prefrontal cortex, and pregenual cingulate cortex.

The Matrix of the Connectivity of the Eight OFC and Related Areas

Figure 4 shows a matrix of the connectivity measured across the 50 participants for the 18 AAL3 regions in the 8 ROIs (left and right vmPFC [FrontalMedOrb], medOFC [Rectus, OFCmed, OFCant, and OFCpost], latOFClat [OFClat and IFGorb], and IFG [IFGoperc and IFGtri]) with other ipsilateral AAL3 brain regions. The connectivity of these 18 ROIs is typically greater ipsilaterally than contralaterally (with the contralateral connectivity shown in Supplementary Fig. S2), and for most ROIs apart from the IFG, the connectivity is approximately symmetric in the two hemispheres.

Figure 4 (top row for the left and right connectivity matrices) shows that the ventromedial prefrontal cortex has strong direct connectivity with medial OFC areas (especially with OFCmed and OFCpost), the caudate and putamen, the subgenual anterior cingulate cortex, temporal cortical areas, and some connectivity with superior and middle frontal gyri, the orbital part of the inferior frontal gyrus and lateral OFC, and the insula.

The medial OFC (AAL3 areas rectus, OFCmed, OFCant, and OFCpost) have strong direct connectivity with the ventromedial prefrontal cortex, striatum especially the ventral striatum, the anterior cingulate cortex especially the subgenual part, temporal cortical areas, and some connectivity with superior and middle frontal gyri and the orbital part of the inferior frontal gyrus. Differences between these AAL3 areas are that the OFCpost has especially strong connections with other parts of the medial OFC (including rectus, OFCmed, and OFC ant), with the vmPFC, with the orbital part of the inferior frontal gyrus (and the connected OFClat), and with the superior and middle frontal gyri. The post-OFC is thus notable as being highly connected, like a hub. The rectus and OFCmed have especially strong connections with the nucleus accumbens and olfactory tubercle, which comprise the ventral striatum.

The lateral OFC (AAL3 areas OFClat and IFGorb) has direct connectivity with the inferior frontal gyrus, superior, middle, and medial superior prefrontal areas, the posterior OFC, insula, caudate and putamen with less connectivity with the ventral striatum, temporal cortex, and supramarginal and inferior parietal cortical areas. The IFGorb has a stronger connectivity with parietal areas than OFClat.

The rIFG (AAL3 areas R.IFGoperc and R.IFGtri) has direct connections with many right prefrontal cortical areas, right premotor (precentral gyrus and supplementary motor area), postcentral cortex and midcingulate cortex, supracallosal anterior

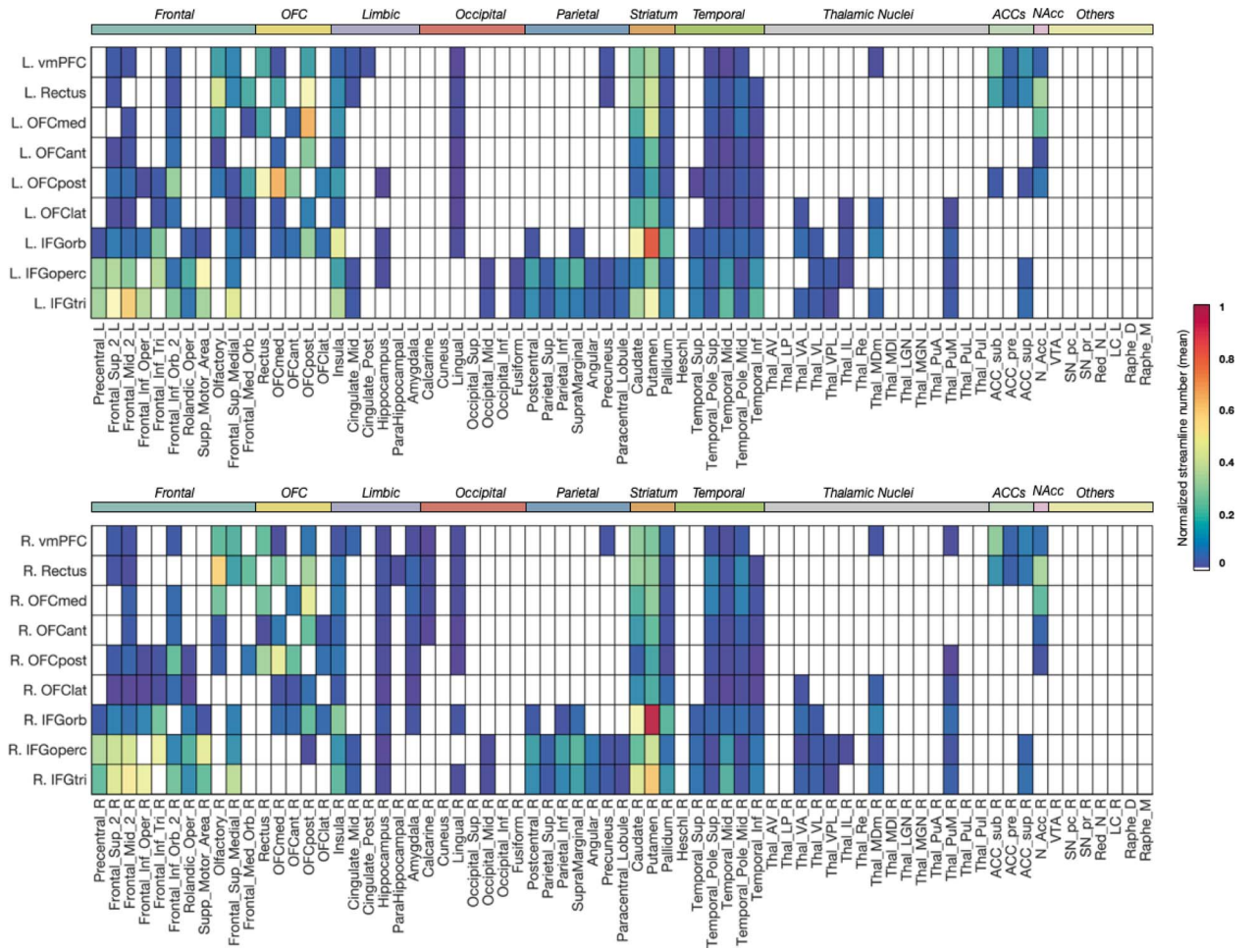

Figure 4. Matrix of connectivity across the 50 participants for each of the 18 AAL3 areas in the 8 ROIs, (left and right) ventromedial prefrontal cortex (FrontalMedOrb), medial OFC (rectus, OFCmed, OFCant, and OFCpost), lateral OFC (OFClat and IFGorb), and inferior frontal gyrus (IFGtri and IFGoperc) with each ipsilateral AAL3 area. Only significant connections are shown, tested as described in Materials and Methods. The connectivity matrix shows the 140 areas in the AAL3 atlas excluding the cerebellar areas. The names of the AAL3 areas are shown in Supplementary Tables S1 and S2. The contralateral connectivity is shown in Figure S2.

cingulate cortex, and right supramarginal, angular, and inferior parietal cortical areas.

The left inferior frontal gyrus has direct connections with many left prefrontal cortical areas; left premotor, postcentral cortex, and midcingulate cortex; supracallosal anterior cingulate cortex; and left supramarginal, angular, and inferior parietal cortical areas.

The connections shown in Figure 4 can be summarized in another way, by considering the connectivities of OFC/IFG subregions with different brain systems. The temporal cortical areas are connected with all of these OFC/IFG regions. The parietal areas including the supramarginal and angular gyri are connected especially with the inferior frontal gyri, and not with the OFC and vmPFC. The IFGorb appears to have similarities with the other IFG areas and with the OFClat and may be an intermediate area. The subgenual and pregenual anterior cingulate cortex tend to be connected with the medial OFC and vmPFC areas, whereas the supracallosal anterior cingulate cortex tends to be more connected with the inferior frontal gyrus areas including IFGorb. The posterior cingulate cortex and precuneus are especially connected with the vmPFC and the gyrus rectus. Motor areas, such as the precentral gyrus, supplementary motor area, rolandic operculum, and midcingulate cortex, are connected with the IFG but much less with the OFC and vmPFC. The ventral striatum (NAcc and olfactory tubercle) are connected especially with the medial OFC and vmPFC. The superior and middle frontal gyri appear to be connected with all OFC, vmPFC, and IFG areas.

Figure 5 shows the correlation between the connectivity of each of the 18 AAL3 areas with all ipsilateral AAL3 brain areas across 50 participants. The medial orbitofrontal areas rectus, OFCmed and OFCant, and the vmPFC form one group that have high correlations with each other. They have moderately high correlations with the pregenual and subgenual anterior cingulate cortex. Within this group, the vmPFC and gyrus rectus have especially strong correlations with the anterior cingulate cortex. The OFCpost forms a second group, and stands out as having connectivity that is different from most of these OFC, IFG, and vmPFC areas, perhaps because it is a hub region. The OFClat and IFGorb form a third group, with connectivity correlated with that of medial OFC areas, which is not the case for the fourth group, IFGtri and IFGoperc. The fourth group, IFGtri and IFGoperc, have similar connectivity to parietal areas including the supramarginal and angular gyri and precuneus; to temporal

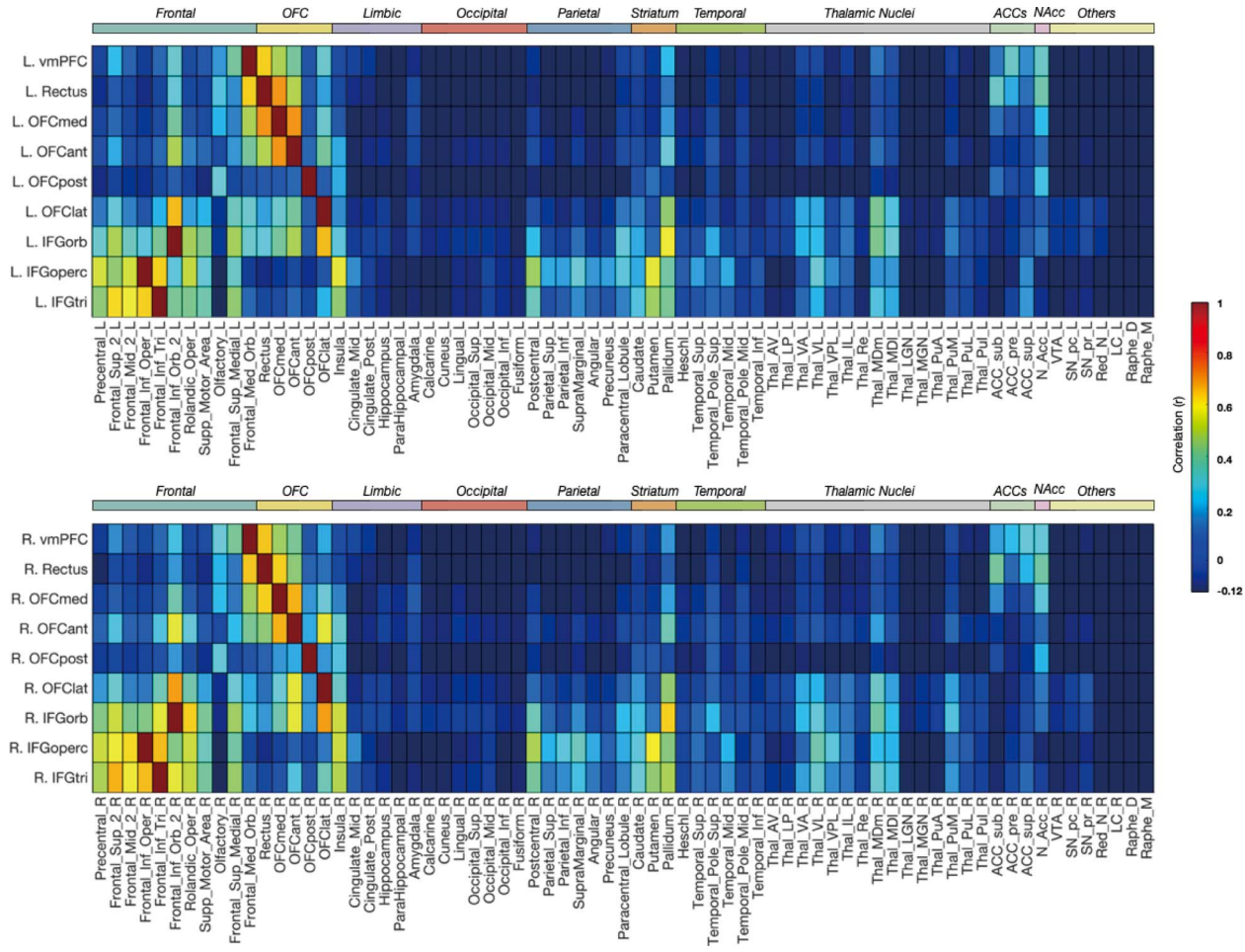

Figure 5. The Pearson correlation matrix between the connectivity of each of the 18 AAL3 areas in the 8 ROIs with all ipsilateral AAL3 brain areas across 50 participants.

lobe areas; to prefrontal areas including the superior and middle frontal gyri; and to some motor areas, including the precentral gyrus, supplementary motor area, Rolandic operculum, and mid-cingulate cortex. The connectivity of the lateral OFC is correlated with that of the inferior frontal gyrus on the same side of the brain, and interestingly, these connectivities had low correlations between the two hemispheres. This is an indication that the left and right lateral orbitofrontal may have different functions (Supplementary Fig. S3). These groups defined by the correlations shown in Figure 5 are of interest, for they help to define anatomical networks with similar connectivity (and implied interconnectivity within a network) in the human brain.

Figure 6 shows a multidimensional scaling (MDS) space for the 18 AAL3 areas, based on their anatomical connectivity with AAL3 brain areas from Supplementary Figure S2. Figure 6 is for when the AAL3 areas are from both hemispheres, and very similar results were found when the AAL3 areas were only from the ipsilateral hemisphere. Figure 6 shows that the OFCmed, OFCant, gyrus rectus, and vmPFC are relatively close together in one part of the space, reflecting their similar connectivity with all AAL3 areas. The OFClat and IFGorb are relatively close to each other, indicating their similar connectivity to each other. Their position in the space is intermediate between the medial OFC areas and the IFG areas, which form a third part of the space. The OFCpost is separate in the space. This supports the points made when considering the results in Figure 5 that there are four main groups of regions among the 18 AAL3 areas considered. The pattern of left and right anatomical connectivities is similar, as shown by the closeness of the right and left corresponding AAL3 areas in this space.

Tractography

We provide tractography diagrams for five ROIs in the OFC (Supplementary Fig. S4), ventromedial prefrontal cortex, and inferior frontal gyrus of one representative participant. The overall pattern shows prominent interhemispheric connections of the five regions. The tractography for both the right and left IFG shows connections with the superior and middle temporal regions via the arcuate fasciculus.

Discussion

One key finding is that the human medial and lateral OFC have different direct connections with other parts of the brain. The medial OFC has direct connections with the anterior cingulate cortex including the pregenual and subgenual parts (Fig. 4); all of which are reward-related areas (Rolls 2019b, 2019c). The lateral OFC has fewer connections with these parts of the anterior cingulate cortex, but the inferior frontal gyrus (which especially

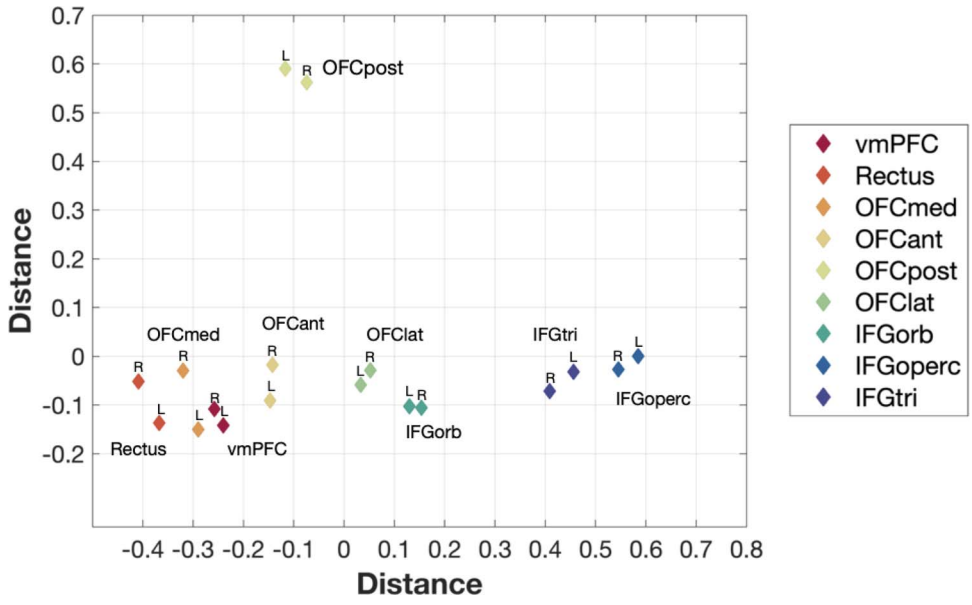

Figure 6. MDS to enable the visualization of the distances between the connectivity of the 18 ROIs with all AAL3 regions. The data were from the connectivity matrix shown in Supplementary Figure S2. The connections of any one ROI in this diagram with all AAL3 regions, whether on the Left or Right, are shown. The results were similar if the connections with ipsilateral AAL3 areas were used. Distances in this space reflect the dissimilarity of the connectivity.

on the right is related to the lateral OFC) has direct connections with the supracallosal anterior cingulate cortex (Fig. 4); all of which are punishment or nonreward-related areas (Rolls 2019b, 2019c). This extends the evidence from functional connectivity about the relations between these different parts of the medial OFC versus lateral OFC and its closely related rIFG (Rolls et al. 2019; Du et al. 2020), by adding evidence about direct connections. This is consistent with the hypotheses that the OFC computes reward value and thereby is related to emotion and that the anterior cingulate cortex provides a route to goal-related actions (Rolls 2019a).

A second key finding is that the lateral OFC and rIFG direct connections are somewhat similar to each other and somewhat different from medial OFC areas, in terms of their direct connections with right hemisphere parietal areas, such as the supramarginal gyrus and inferior parietal cortex (Fig. 4), and also some movement-related areas, such as the supplementary motor cortex. This is consistent with the hypothesis that the lateral OFC and the associated rIFG provide routes to behavioral output for the OFC (Du et al. 2020) which have greater functional connectivity in depression (Rolls, Cheng, et al. 2020a). This extends the nonreward attractor theory of depression (Rolls 2016b) beyond the lateral OFC to include at least parts of the rIFG. A concept here is that with the involvement of the left inferior frontal gyrus in language (as Broca's area (Amunts and Zilles 2012; Clos et al. 2013)), the left OFC becomes constrained in size, whereas the rIFG can be more involved in the functions of the right OFC, for which the right IFG may provide a route to output (Rolls, Cheng, et al. 2020a).

Another key finding is that the ventromedial prefrontal cortex shares with the medial OFC especially strong outputs to the nucleus accumbens and olfactory tubercle, which comprise the ventral striatum, whereas the other ROIs have more widespread outputs to the striatum (Fig. 4). In macaques, the OFC also projects to the ventral striatum (Selemon and Goldman-Rakic 1985; Yeterian and Pandya 1991; Haber et al. 1995; Haber 2016) (which helps to validate the current findings), but what is shown in Figure 4 provides quantitative evidence for humans how this is especially the case for the vmPFC and medial OFC, whereas the lateral OFC and inferior frontal gyrus have relatively stronger connections with the caudate nucleus and putamen. The ventromedial prefrontal cortex such as the medial OFC also has strong direct connections with the anterior cingulate cortex, and indeed, the connections with the subgenual and pregenual cingulate cortices distinguish these areas from the other ROIs.

As shown in Figure 4 and summarized in the Results, the connections of the different OFC/IFG AAL3 areas form interesting anatomical groupings. We now show how these anatomical groupings have functional relevance. First, the medial OFC has strong direct connectivity with the pregenual and subgenual anterior cingulate cortex, and both are implicated in reward processing (Grabenhorst and Rolls 2011; Rolls 2019b, 2019c). Conversely, the lateral OFC has strong direct connectivity with the supracallosal anterior cingulate cortex (Fig. 4), and both are implicated in punishment and nonreward processing (Grabenhorst and Rolls 2011; Rolls 2019b, 2019c). This may be a network in which reward and punishment value is computed in the OFC, and this information is sent to the anterior cingulate cortex for action to reward outcome learning (Rolls 2019a). The orbital part of the inferior frontal gyrus (IFGorb) appears to have similarities with both OFClat and the other IFG areas. On the right (i.e., contralateral to the language hemisphere), the orbital part of the inferior frontal gyrus appears to be functionally especially related to increased functional connectivity in depression and may provide a route from the lateral OFC to premotor areas (Cheng et al. 2016; Rolls, Cheng, et al. 2020a).

Second, the posterior cingulate cortex and precuneus are especially connected with the vmPFC and the gyrus rectus. This is especially interesting as both are related to memory, including autobiographical memory (Bonnici and Maguire 2018; McCormick et al. 2018). Consistent with this, the parahippocampal cortex, also with the hippocampus involved in memory (Rolls 2018), is especially connected with the vmPFC and gyrus rectus.

Thus, the vmPFC and gyrus rectus have connections in humans that relate them to memory functions, and this may be a distinct system from the medial and lateral OFC.

Third, the parietal areas including the supramarginal (BA40) and angular gyri (BA39) are connected especially with the inferior frontal gyri, and not with the OFC and vmPFC. On the left, these are key areas involved with language, with the inferior frontal gyrus pars triangularis (BA45) and pars opercularis (BA44) forming Broca's area, and at least the angular gyri and related parieto-temporal areas involved in language and related processing (Amunts and Zilles 2012; DeWitt and Rauschecker 2013; Binder 2015; Campbell and Tyler 2018).

Fourth, motor areas, such as the precentral gyrus, supplementary motor area, Rolandic operculum, and midcingulate cortex, are connected with the IFG but much less with the OFC and vmPFC. The ventral striatum (NAcc and olfactory tubercle) are connected especially with the medial OFC and vmPFC.

Fifth, the temporal cortical areas lobe had connections with all OFC, vmPFC, and IFG areas. What was especially interesting, as shown in Figure 2 and Supplementary Figure S1, is that the connections were especially strong with the temporal pole, though connections were also found less anteriorly. These temporal lobe regions are involved in visual (including face expression), auditory, and semantic functions (Patterson et al. 2007; Cheng et al. 2015; Rolls 2021). Consistent with the findings presented here for humans, in macaques, the medial OFC areas do have strong connectivity with the temporal pole (Corcoles–Parada et al. 2019), and the middle part of the superior temporal gyrus connects to the lateral OFC area 12 and more laterally (Petrides and Pandya 1988). The superior and middle frontal gyri appear to be connected at all OFC, vmPFC, and IFG areas, and these connections may be involved in working memory and executive function (Passingham and Wise 2012).

Sixth, as shown in Figure 4 and supported by Figures 5 and 6, the OFCpost is somewhat more connected than OFCant and other parts of the OFC and appears to be a hub region. Differences are found in the architecture which, for the posterior OFC, is less elaborated than more anteriorly (Beck 1949; Barbas and Pandya 1989; Hof et al. 1995) and, in macaques, is related to different patterns of connections with anterior cingulate (Garcia-Cabezas and Barbas 2017) and other areas (Barbas 1993).

There is an interesting similarity between the direct connections of these ROIs (Figs 2 and 3) and their functional connectivity shown in Figure 2 of Du et al. (2020). Connectivity revealed by the functional connectivity but not by the direct connections includes the angular gyrus with ventromedial prefrontal cortex, medial OFC, and lateral OFC (Du et al. 2020), and these therefore may be trans-synaptic connections. On the other hand, there is a strong functional connectivity of the inferior frontal gyrus with the supramarginal gyrus (Fig. 2 of Du et al. (2020)), and that may be mediated by direct connectivity as shown in Figure 4. In addition, it is interesting to compare Figure 4 with a corresponding figure based on the functional connectivity of parcels within the OFC and related ventromedial and inferior frontal gyrus brain areas (Fig. 4 of (Du et al. 2020)). Both figures emphasize the differences of the connectivity of the vmPFC, medial OFC, lateral OFC, and inferior frontal gyrus.

An important guide to the connectivity of the human OFC is the wealth of evidence available about the macaque OFC (Carmichael and Price 1996; Price 2006, 2007; Barbas 2007; Saleem et al. 2008, 2014; Barbas et al. 2011). However, the findings described here while generally consistent go beyond those studies by providing evidence about the asymmetry of the human right and left lateral OFC and inferior frontal gyri; by highlighting the connections of the human OFC with parietal cortical areas some of which are involved in functions related to language; and in revealing the connectivity of the human medial OFC with the pregenual cingulate cortex, and the lateral OFC with the supracallosal anterior cingulate cortex, areas involved in humans, respectively, in reward versus punishment and nonreward processing (Rolls 2019a, 2019b, 2019c).

In relation to macaque anatomical studies, the connections shown in Figure 4 are of interest, because they are based on a statistical analysis. This is in contrast to most anatomical studies in macaques, which are based essentially on several single case studies, in which particular case studies of injections into individual receiving areas (identified with retrograde tracers such as HRP) or sending areas (using anterograde tracers injected into a particular region) are performed. In contrast, in the present approach, and potentially in future approaches in humans, the anatomical connectivity can be based on the statistical analyses of connectivity between voxels throughout the brain, which is essentially what happened in the present investigation, which then allows networks of connectivity to be defined, identified by statistical analysis, such as correlation as used here (Fig. 5), or potentially further approaches.

In order to obtain more precise fiber orientation estimates and more reliable tractography, the MSMT-CSD algorithm combined with ACT was used in this study (Smith et al. 2012; Jeurissen et al. 2014). However, there are still some limitations that may result in failing to identify particular connections. One limitation can arise for example when there are many tangential fibers to a pathway as described in Introduction, as occurs for example in the dense WM zone where axons run parallel to the cortical surface beneath the infragranular layer (Reveley et al. 2015; Donahue et al. 2016). Because much of the diffusion is in the tangential direction, it is difficult to follow orthogonal streamlines across this region penetrating into the cortex. A similar issue may apply to OFC connections with the amygdala, partly because there are many tangential fibers where the streamlines enter the amygdala, and partly because there may be a sharp turn in the streamlines at the entrance to the amygdala (Solano-Castiella et al. 2010), whereas most tracking algorithms favor the straight option (turning through an angle of less than 60°) (Jeurissen et al. 2019). Thus, while the connectivity between the OFC and amygdala has been well documented in functional connectivity and tracer studies (Carmichael and Price 1995; Ghashghaei and Barbas 2002; Barbas 2007; Garcia-Cabezas and Barbas 2017; Cheng, Rolls, Qiu, Xie, Lyu, et al. 2018a), it was hard to follow the streamlines into the amygdala in this study and in previous diffusion studies (Eden et al. 2015; Gibbard et al. 2018; Rizzo et al. 2018) (though streamlines terminating at the entrance to the amygdala are shown in Figs 2 and 3). Nevertheless, although tractography needs to be treated with caution because of possible false negatives and positives, it has been the only methodology for noninvasively delineating the WM pathways in the human brain. In this study, our purpose was not to provide a novel method to improve the tractography algorithm.

Instead, this study takes the OFC and its related areas, parts of the brain important in emotion and in emotional disorders such as depression, and shows how these areas connect to other key brain regions, adding importantly to what can be assessed by anatomical path tracing studies in nonhuman primates, partly because some of the areas involved are much more developed in humans, including parts of the inferior frontal gyrus and the

angular and supramarginal gyri. The present study also provides interesting evidence on the differences of connectivity of these brain regions, as described above. Moreover, this study provides a foundation for future longitudinal studies and for studies in patients with disorders.

Supplementary Material

Supplementary material can be found at *Cerebral Cortex* online.

Funding

Ministry of Science and Technology (MOST) of Taiwan (grant MOST 109-2634-F-010-001, MOST 108-2321-B-010-013-MY2, MOST 108-2321-B-010-010-MY2 and MOST 108-2420-H-010-001-to C.P.L.); Taiwan National Health Research Institutes (grant NHRI-EX108-10611EI to C.P.L.); Shanghai Science and Technology Innovation Plan (grant 17JC1404105, 17JC1404101 to C.P.L., and 16JC1420402 to J.F.); National Key Research and Development Program of China (grant 2018YFC0910503 to C.Y.L., and 2018YFC1312900 and 2019YFA0709502 to J.F.); The Young Scientists Fund of the National Natural Science Foundation of China (grant 81801774 to C.Y.L.); Natural Science Foundation of Shanghai (grant 18ZR1403700 to C.Y.L); Shanghai Municipal Science and Technology Major Project (grant 2018SHZDZX01 to C.Y.L and J.F.); The Zhangjiang Lab (to J.F.); 111 project (grant B18015 to J.F.); National Natural Science Foundation of China (grant 91630314 to J.F.); The Shanghai AI Platform for Diagnosis and Treatment of Brain Diseases (to J.F.).

Notes

This work was supported in part by the Brain Research Center, National Yang-Ming University from The Featured Areas Research Center Program within the framework of the Higher Education Sprout Project by the Ministry of Education (MOE) in Taiwan (to C.P.L.). The authors also acknowledge MRI support from the MRI Core of National Yang-Ming University, Taiwan. *Conflict of Interest:* None declared.

References

Amunts K, Zilles K. 2012. Architecture and organizational principles of Broca's region. *Trends Cogn Sci*. 16:418–426.

Barbas H. 1993. Organization of cortical afferent input to the orbitofrontal area in the rhesus monkey. *Neuroscience*. 56:841–864.

Barbas H. 2007. Specialized elements of orbitofrontal cortex in primates. *Ann N Y Acad Sci*. 1121:10–32.

Barbas H, Pandya DN. 1989. Architecture and intrinsic connections of the prefrontal cortex in the rhesus monkey. *J Comp Neurol*. 286:353–375.

Barbas H, Zikopoulos B, Timbie C. 2011. Sensory pathways and emotional context for action in primate prefrontal cortex. *Biol Psychiatry*. 69:1133–1139.

Beck E. 1949. A cytoarchitectural investigation into the boundaries of cortical areas 13 and 14 in the human brain. *J Anat*. 83:147–157.

Binder JR. 2015. The Wernicke area: modern evidence and a reinterpretation. *Neurology*. 85:2170–2175.

Bonnici HM, Maguire EA. 2018. Two years later—revisiting autobiographical memory representations in vmPFC and hippocampus. *Neuropsychologia*. 110:159–169.

Campbell KL, Tyler LK. 2018. Language-related domain-specific and domain-general systems in the human brain. *Curr Opin Behav Sci*. 21:132–137.

Carmichael ST, Price JL. 1995. Limbic connections of the orbital and medial prefrontal cortex in macaque monkeys. *J Comp Neurol*. 363:615–641.

Carmichael ST, Price JL. 1996. Connectional networks within the orbital and medial prefrontal cortex of macaque monkeys. *J Comp Neurol*. 371:179–207.

Catani M, Dell'acqua F, Thiebaut de Schotten M. 2013. A revised limbic system model for memory, emotion and behaviour. *Neurosci Biobehav Rev*. 37:1724–1737.

Cheng W, Rolls ET, Gu H, Zhang J, Feng J. 2015. Autism: reduced functional connectivity between cortical areas involved in face expression, theory of mind, and the sense of self. *Brain*. 138:1382–1393.

Cheng W, Rolls ET, Qiu J, Liu W, Tang Y, Huang CC, Wang X, Zhang J, Lin W, Zheng L *et al*. 2016. Medial reward and lateral non-reward orbitofrontal cortex circuits change in opposite directions in depression. *Brain*. 139: 3296–3309.

Cheng W, Rolls ET, Qiu J, Xie X, Lyu W, Li Y, Huang CC, Yang AC, Tsai SJ, Lyu F *et al*. 2018a. Functional connectivity of the human amygdala in health and in depression. *Soc Cogn Affect Neurosci*. 13:557–568.

Cheng W, Rolls ET, Qiu J, Xie X, Wei D, Huang CC, Yang AC, Tsai SJ, Li Q, Meng J *et al*. 2018b. Increased functional connectivity of the posterior cingulate cortex with the lateral orbitofrontal cortex in depression. *Transl Psychiatry*. 8:90.

Cheng W, Rolls ET, Qiu J, Yang D, Ruan H, Wei D, Zhao L, Meng J, Xie P, Feng J. 2018c. Functional connectivity of the precuneus in unmedicated patients with depression. *Biol Psychiatry Cogn Neurosci Neuroimaging*. 3:1040–1049.

Cheng W, Rolls ET, Ruan H, Feng J. 2018d. Functional connectivities in the brain that mediate the association between depressive problems and sleep quality. *JAMA Psychiat*. 75:1052–1061.

Clos M, Amunts K, Laird AR, Fox PT, Eickhoff SB. 2013. Tackling the multifunctional nature of Broca's region meta-analytically: co-activation-based parcellation of area 44. *Neuroimage*. 83:174–188.

Corcoles-Parada M, Ubero-Martinez M, Morris RGM, Insausti R, Mishkin M, Munoz-Lopez M. 2019. Frontal and insular input to the dorsolateral temporal pole in primates: implications for auditory memory. *Front Neurosci*. 13:1099.

DeWitt I, Rauschecker JP. 2013. Wernicke's area revisited: parallel streams and word processing. *Brain Lang*. 127: 181–191.

Donahue CJ, Sotiropoulos SN, Jbabdi S, Hernandez-Fernandez M, Behrens TE, Dyrby TB, Coalson T, Kennedy H, Knoblauch K, Van Essen DC *et al*. 2016. Using diffusion tractography to predict cortical connection strength and distance: a quantitative comparison with tracers in the monkey. *J Neurosci*. 36:6758–6770.

Du J, Rolls ET, Cheng W, Li Y, Gong W, Qiu J, Feng J. 2020. Functional connectivity of the orbitofrontal cortex, anterior cingulate cortex, and inferior frontal gyrus in humans. *Cortex*. 123:185–199.

Eden AS, Schreiber J, Anwander A, Keuper K, Laeger I, Zwanzger P, Zwitserlood P, Kugel H, Dobel C. 2015. Emotion regulation and trait anxiety are predicted by the microstructure of fibers between amygdala and prefrontal cortex. *J Neurosci*. 35:6020–6027.

Folloni D, Sallet J, Khrapitchev AA, Sibson N, Verhagen L, Mars RB. 2019. Dichotomous organization of amygdala/temporal-prefrontal bundles in both humans and monkeys. *Elife*. 8:e47175.

Garcia-Cabezas MA, Barbas H. 2017. Anterior cingulate pathways may affect emotions through orbitofrontal cortex. *Cereb Cortex*. 27:4891–4910.

Ghashghaei HT, Barbas H. 2002. Pathways for emotion: interactions of prefrontal and anterior temporal pathways in the amygdala of the rhesus monkey. *Neuroscience*. 115:1261–1279.

Gibbard CR, Ren J, Skuse DH, Clayden JD, Clark CA. 2018. Structural connectivity of the amygdala in young adults with autism spectrum disorder. *Hum Brain Mapp*. 39:1270–1282.

Glascher J, Adolphs R, Damasio H, Bechara A, Rudrauf D, Calamia M, Paul LK, Tranel D. 2012. Lesion mapping of cognitive control and value-based decision making in the prefrontal cortex. *Proc Natl Acad Sci U S A*. 109:14681–14686.

Grabenhorst F, Rolls ET. 2011. Value, pleasure, and choice in the ventral prefrontal cortex. *Trends Cogn Sci*. 15:56–67.

Greve DN, Fischl B. 2009. Accurate and robust brain image alignment using boundary-based registration. *Neuroimage*. 48:63–72.

Haber SN. 2016. Corticostriatal circuitry. *Dialogues Clin Neurosci*. 18:7–21.

Haber SN, Kunishio K, Mizobuchi M, Lynd-Balta E. 1995. The orbital and medial prefrontal circuit through the primate basal ganglia. *J Neurosci*. 15:4851–4867.

Hof PR, Mufson EJ, Morrison JH. 1995. Human orbitofrontal cortex: cytoarchitecture and quantitative immunohistochemical parcellation. *J Comp Neurol*. 359:48–68.

Hornak J, O'Doherty J, Bramham J, Rolls ET, Morris RG, Bullock PR, Polkey CE. 2004. Reward-related reversal learning after surgical excisions in orbitofrontal and dorsolateral prefrontal cortex in humans. *J Cogn Neurosci*. 16:463–478.

Jenkinson M, Bannister P, Brady M, Smith S. 2002. Improved optimization for the robust and accurate linear registration and motion correction of brain images. *Neuroimage*. 17:825–841.

Jenkinson M, Smith S. 2001. A global optimisation method for robust affine registration of brain images. *Med Image Anal*. 5:143–156.

Jeurissen B, Descoteaux M, Mori S, Leemans A. 2019. Diffusion MRI fiber tractography of the brain. *NMR Biomed*. 32:e3785.

Jeurissen B, Tournier JD, Dhollander T, Connelly A, Sijbers J. 2014. Multi-tissue constrained spherical deconvolution for improved analysis of multi-shell diffusion MRI data. *Neuroimage*. 103:411–426.

Johansen-Berg H, Behrens TE, Sillery E, Ciccarelli O, Thompson AJ, Smith SM, Matthews PM. 2005. Functional-anatomical validation and individual variation of diffusion tractography-based segmentation of the human thalamus. *Cereb Cortex*. 15:31–39.

Johansen-Berg H, Gutman DA, Behrens TE, Matthews PM, Rushworth MF, Katz E, Lozano AM, Mayberg HS. 2008. Anatomical connectivity of the subgenual cingulate region targeted with deep brain stimulation for treatment-resistant depression. *Cereb Cortex*. 18:1374–1383.

McCormick C, Ciaramelli E, De Luca F, Maguire EA. 2018. Comparing and contrasting the cognitive effects of hippocampal and ventromedial prefrontal cortex damage: a review of human lesion studies. *Neuroscience*. 374:295–318.

Mori S, van Zijl PC. 2002. Fiber tracking: principles and strategies - a technical review. *NMR Biomed*. 15:468–480.

Nasreddine ZS, Phillips NA, Bedirian V, Charbonneau S, Whitehead V, Collin I, Cummings JL, Chertkow H. 2005. The Montreal cognitive assessment, MoCA: a brief screening tool for mild cognitive impairment. *J Am Geriatr Soc*. 53:695–699.

Öngür D, Ferry AT, Price JL. 2003. Architectonic division of the human orbital and medial prefrontal cortex. *J Comp Neurol*. 460:425–449.

Passingham REP, Wise SP. 2012. *The neurobiology of the prefrontal cortex*. Oxford: Oxford University Press.

Patterson K, Nestor PJ, Rogers TT. 2007. Where do you know what you know? The representation of semantic knowledge in the human brain. *Nat Rev Neurosci*. 8:976–987.

Petrides M, Pandya DN. 1988. Association fiber pathways to the frontal cortex from the superior temporal region in the rhesus monkey. *J Comp Neurol*. 273:52–66.

Price JL. 2006. Connections of orbital cortex. In: Zald DH, Rauch SL, editors. *The orbitofrontal cortex*. Oxford: Oxford University Press, pp. 39–55.

Price JL. 2007. Definition of the orbital cortex in relation to specific connections with limbic and visceral structures and other cortical regions. *Ann N Y Acad Sci*. 1121:54–71.

Reveley C, Seth AK, Pierpaoli C, Silva AC, Yu D, Saunders RC, Leopold DA, Ye FQ. 2015. Superficial white matter fiber systems impede detection of long-range cortical connections in diffusion MR tractography. *Proc Natl Acad Sci U S A*. 112:E2820–E2828.

Rizzo G, Milardi D, Bertino S, Basile GA, Di Mauro D, Calamuneri A, Chillemi G, Silvestri G, Anastasi G, Bramanti A *et al*. 2018. The limbic and sensorimotor pathways of the human amygdala: a structural connectivity study. *Neuroscience*. 385:166–180.

Rolls ET. 2014. *Emotion and decision-making explained*. Oxford: Oxford University Press.

Rolls ET. 2016a. *Cerebral cortex: principles of operation*. Oxford: Oxford University Press.

Rolls ET. 2016b. A non-reward attractor theory of depression. *Neurosci Biobehav Rev*. 68:47–58.

Rolls ET. 2018. The storage and recall of memories in the hippocampo-cortical system. *Cell Tissue Res*. 373:577–604.

Rolls ET. 2019a. The cingulate cortex and limbic systems for emotion, action, and memory. *Brain Struct Funct*. 224:3001–3018.

Rolls ET. 2019b. *The orbitofrontal cortex*. Oxford: Oxford University Press.

Rolls ET. 2019c. The orbitofrontal cortex and emotion in health and disease, including depression. *Neuropsychologia*. 128:14–43.

Rolls ET. 2021. *Brain computations: a systems-level analysis*. Oxford: Oxford University Press.

Rolls ET, Cheng W, Du J, Wei D, Qiu J, Dai D, Zhou Q, Xie P, Feng J. 2020a. Functional connectivity of the right inferior frontal gyrus and orbitofrontal cortex in depression. *Soc Cogn Affect Neurosci*. 15:75–86.

Rolls ET, Cheng W, Gong W, Qiu J, Zhou C, Zhang J, Lv W, Ruan H, Wei D, Cheng K *et al*. 2019. Functional connectivity of the anterior cingulate cortex in depression and in health. *Cereb Cortex*. 29:3617–3630.

Rolls ET, Grabenhorst F. 2008. The orbitofrontal cortex and beyond: from affect to decision-making. *Prog Neurobiol*. 86:216–244.

Rolls ET, Grabenhorst F, Deco G. 2010a. Choice, difficulty, and confidence in the brain. *Neuroimage*. 53:694–706.

Rolls ET, Grabenhorst F, Deco G. 2010b. Decision-making, errors, and confidence in the brain. *J Neurophysiol*. 104: 2359–2374.

Rolls ET, Huang CC, Lin CP, Feng J, Joliot M. 2020b. Automated anatomical labelling Atlas 3. *Neuroimage*. 206: 116189.

Rolls ET, Joliot M, Tzourio-Mazoyer N. 2015. Implementation of a new parcellation of the orbitofrontal cortex in the automated anatomical labeling Atlas. *Neuroimage*. 122:1–5.

Saleem KS, Kondo H, Price JL. 2008. Complementary circuits connecting the orbital and medial prefrontal networks with the temporal, insular, and opercular cortex in the macaque monkey. *J Comp Neurol*. 506:659–693.

Saleem KS, Miller B, Price JL. 2014. Subdivisions and connectional networks of the lateral prefrontal cortex in the macaque monkey. *J Comp Neurol*. 522:1641–1690.

Selemon LD, Goldman-Rakic PS. 1985. Longitudinal topography and interdigitation of corticostriatal projections in the rhesus monkey. *J Neurosci*. 5:776–794.

Smith RE, Tournier JD, Calamante F, Connelly A. 2012. Anatomically-constrained tractography: improved diffusion MRI streamlines tractography through effective use of anatomical information. *Neuroimage*. 62:1924–1938.

Smith SM. 2002. Fast robust automated brain extraction. *Hum Brain Mapp*. 17:143–155.

Solano-Castiella E, Anwander A, Lohmann G, Weiss M, Docherty C, Geyer S, Reimer E, Friederici AD, Turner R. 2010. Diffusion tensor imaging segments the human amygdala in vivo. *Neuroimage*. 49:2958–2965.

Tournier J-D, Calamante F, Connelly A. 2010. Improved probabilistic streamlines tractography by 2nd order integration over fibre orientation distributions. *Proc Intl Soc Mag Reson Med (ISMRM)*. 18:1670.

Van Essen DC, Hayashi T, Autio J, Ose T, Nishigori K, Coalsor T, Hou Y, Smith S, Shen Z, Knoblauch K *et al*. 2019. Evaluation of functional connectivity using retrograde tracers in the macaque monkey. *OHBM*. https://www.pathlms.com/ohbm/courses/12238/sections/15845/video_presentations/138035 (last accessed date April 2020).

Wheeler EZ, Fellows LK. 2008. The human ventromedial frontal lobe is critical for learning from negative feedback. *Brain*. 131:1323–1331.

Yeterian EH, Pandya DN. 1991. Prefrontostriatal connections in relation to cortical architectonic organization in rhesus monkeys. *J Comp Neurol*. 312:43–67.

Zajac L, Koo BB, Bauer CM, Killiany R, Behalf Of The Alzheimer's Disease Neuroimaging I. 2017. Seed location impacts whole-brain structural network comparisons between healthy elderly and individuals with Alzheimer's disease. *Brain Sci*. 7:37.